Lithos xxx (2009) xxx–xxx

Contents lists available at ScienceDirect

Lithos

journal homepage: www.elsevier.com/locate/lithos

# Carbonate assimilation in magmas: A reappraisal based on experimental petrology

Silvio Mollo [a,*], Mario Gaeta [a,b], Carmela Freda [a], Tommaso Di Rocco [b], Valeria Misiti [a], Piergiorgio Scarlato [a]

[a] Istituto Nazionale di Geofisica e Vulcanologia, Via di Vigna Murata 605 00143 Rome, Italy
[b] Dipartimento di Scienze della Terra, Sapienza Università di Roma, P.le Aldo Moro 5 00176 Rome, Italy

ARTICLE INFO

*Article history:*
Received 18 May 2009
Accepted 2 October 2009
Available online xxxx

*Keywords:*
Carbonate assimilation
Skarn
Redox state
Partition coefficients
Thermo-barometric equation

ABSTRACT

The main effect of magma–carbonate interaction on magma differentiation is the formation of a silica-undersaturated, alkali-rich residual melt. Such a desilication process was explained as the progressive dissolution of $CaCO_3$ in melt by consumption of $SiO_2$ and MgO to form diopside *sensu stricto*. Magma chambers emplaced in carbonate substrata, however, are generally associated with magmatic skarns containing clinopyroxene with a high Ca-Tschermak activity in their paragenesis. Data are presented from magma–carbonate interaction experiments, demonstrating that carbonate assimilation is a complex process involving more components than so far assumed. Experimental results show that, during carbonate assimilation, a diopside–hedenbergite–Ca-Tschermak clinopyroxene solid solution is formed and that Ca-Tschermak/diopside and hedenbergite/diopside ratios increase as a function of the progressive carbonate assimilation. Accordingly, carbonate assimilation reaction should be written as follows, taking into account all the involved magmatic components:

$$CaCO_3^{solid} + SiO_2^{melt} + MgO^{melt} + FeO^{melt} + Al_2O_3^{melt} \rightarrow (Di\text{–}Hd\text{–}CaTs)_{ss}^{solid} + CO_2^{fluid}$$

The texture of experimental products demonstrates that carbonate assimilation produces three-phases (solid, melt, and fluid) whose main products are: i) diopside–hedenbergite–Ca-Tschermak clinopyroxene solid solution; ii) silica-undersaturated CaO-rich melt; and iii) C–O–H fluid phase. The silica undersaturation of the melt and, more importantly, the occurrence of a $CO_2$-rich fluid phase, must be taken into account as they significantly affect partition coefficients and the redox state of carbonated systems, respectively.



## 1. Introduction

Recent petrological and experimental studies have constrained the effect of magma–carbonate interaction on the evolution of magmas (Wenzel et al. 2002; Barnes et al. 2005; Chadwick et al., 2007; Coulson et al., 2007; Freda et al., 2008; Iacono Marziano et al., 2008; Gaeta et al., 2009). These investigations have documented that magma contamination is marked by an abundant crystallization of Ca-rich minerals (mainly clinopyroxene) that affect the stability of liquidus phases (mainly olivine). Consequently, magma becomes progressively depleted in silica and enriched in alkalis (Barnes et al. 2005; Freda et al., 2008; Iacono Marziano et al., 2008).

The desilication reaction was schematised as follow (cf., Iacono Marziano et al., 2008): $CaCO_3^{solid} + SiO_2^{melt} + MgO^{melt} \rightarrow Diopside^{solid} + CO_2^{fluid}$. According to this simplified reaction, the dissolution of $CaCO_3$ in silicate melts results in the progressive formation of silica-undersaturated melts by consuming $SiO_2$ to form diopside, thus implying that the extent of carbonate assimilation is controlled by the MgO content in the melt composition.

Magma chambers emplaced in carbonate substrata are generally associated with cumulates and skarns showing clinopyroxene with high Ca-Tschermak-activity (Gaeta et al., 2009 and references therein). Some of these skarn rocks are characterised by the presence of glass, indicating high-temperature formation. These rocks, progressively grading into a cumulate reaction zone (Beard et al., 2005; Gaeta et al., 2009), must be considered magmatic rather than metasomatic skarns (Kerrick, 1977; Fulignati et al., 2004). On the basis of microtextural observations, mineral chemistry and geochemical data, Gaeta et al. (2009) have demonstrated that rocks characterised by Ca-Tschermak-rich clinopyroxene (i.e., magmatic skarns) can act as a source of CaO-rich silicate melt and that the assimilation of this melt is the process responsible for magma contamination, rather than the ingestion of carbonate wall-rocks. Therefore, the carbonate assimilation reaction should take into account, among reactants, not only MgO but also other magmatic components (e.g., $Al_2O_3$).

In this paper we present new data from magma–carbonate interaction experiments that provide a better understanding of the carbonate assimilation process. Our work highlights the changes in

* Corresponding author.
*E-mail address:* mollo@ingv.it (S. Mollo).

0024-4937/$ – see front matter © 2009 Elsevier B.V. All rights reserved.
doi:10.1016/j.lithos.2009.10.013

textural features, phase chemistry, redox state, and equilibrium conditions induced by magma–carbonate interaction. The information allows us to reappraise the carbonate assimilation reaction which has implications for the application of thermo-barometers to skarn rocks.

## 2. Experimental conditions and analytical methods

The starting material used in this study is a synthetic glass ($SiO_2 = 48.3$, $TiO_2 = 0.7$, $Al_2O_3 = 11.4$, $FeO = 7.5$, $MgO = 13.7$, $CaO = 14$, $Na_2O = 1.2$, $K_2O = 3.3$ [all wt.%]) representative of the most primitive K-basalt outcropping at the Roman Province (Rogers et al., 1985; Kamenetsky et al., 1995; Peccerillo, 2005; Conte et al., 2009).

Starting glass was produced at the Institute for Mineralogy (Leibniz University of Hannover, Germany) from synthetic oxide and carbonate powders. The oxide powder mixture was fused in Pt crucible at 1600 °C, 1 atm, and air $fO_2$. The resulting glass was removed from the Pt crucible, ground and re-melted under the same conditions. To avoid alkali loss, melting duration did not exceed 1.5 h. Backscattered images and microprobe analyses (see below) performed on chips extracted from top, middle, and bottom of the glass, demonstrated homogeneity and the absence crystalline phases.

Experiments were conducted in a 3/4inch piston cylinder at the Bayerisches Geoinstitut (Bayreuth, Germany) and at the HP–HT Laboratory of Experimental Volcanology and Geophysics (Istituto Nazionale di Geofisica e Vulcanologia, Roma, Italy) at 0.5 GPa and various temperatures. The purpose of the experiments was to unravel carbonate assimilation processes occurring at a magma-chamber/wall-rock interface. Therefore, in order to mimic interaction between hot magma and cold carbonate-wall rock, charges were heated from room temperature up to the experimental temperature and held for the experimental duration (Table 1). Three sets of experiments were performed by using the anhydrous starting materials doped with different combinations of $H_2O$ and $CaCO_3$ powder (Massa Carrara pure marble): i) anhydrous glass plus about 1 wt.% of $H_2O$, added by microsyringe directly into the charge; ii) anhydrous glass mixed with $CaCO_3$ powder (5, 10 and 20 wt.%) plus about 1 wt.% of $H_2O$, added by microsyringe; iii) anhydrous glass mixed with 10 wt.% of $CaCO_3$ powder plus about 5 wt.% of $H_2O$, added by microsyringe. In order to investigate the role played by water and dolomite on phase relations and mineral chemistry, one additional run was performed at 0.5 GPa and 1150 °C by doping the starting composition with about 1 wt.% of $H_2O$ and 10 wt.% of powdered $CaMg(CO_3)_2$. Stoichiometry of the used dolomite corresponds to 55.07 and 51.37 mol of CaO and MgO, respectively.

Experimental products were analysed at the HP–HT Laboratory of Experimental Volcanology and Geophysics. Chemical analyses were performed with a Jeol-JXA8200 EDS-WDS combined electron microprobe equipped with five wavelength-dispersive spectrometers, using 15 kV accelerating voltage and 10 nA beam current. Glasses were analysed with a defocused electron beam of 5 μm and a counting time of 5 s on background and 15 s on peak. Whereas for crystals, a beam size of 2 μm and counting time of 20 and 10 s on peaks and background were used respectively. The following standards have been adopted for the various chemical elements: jadeite (Si and Na), corundum (Al), forsterite (Mg), andradite (Fe), rutile (Ti), orthoclase (K), barite (Ba), apatite (P) and spessartine (Mn). Sodium and potassium have been analyzed first to reduce possible volatilization effects.

**Table 1**
Run conditions and phases occurring in experimental products.

| Run # | $P$ (GPa) | $T$ (°C) | Time (h) | Phases (wt.%) |
|---|---|---|---|---|
| *1 wt.% $H_2O$* | | | | |
| 2 | 0.5 | 1200 | 6 | (1)Ol + (99)G |
| 9 | 0.5 | 1150 | 24 | (10)Ol + (44)Cpx + (1)Phl + (45)G |
| *5 wt.% $CaCO_3$ + 1 wt.% $H_2O$* | | | | |
| 14 | 0.5 | 1300 | 21 | (100)G |
| 6 | 0.5 | 1200 | 24 | (8)Ol + (41)Cpx + (1)Phl + (50)G |
| 8 | 0.5 | 1150 | 24 | (9)Ol + (60)Cpx + (1)Phl + (30)G |
| *10 wt.% $CaCO_3$ + 1 wt.% $H_2O$* | | | | |
| 13 | 0.5 | 1300 | 6 | (100)G |
| 15 | 0.5 | 1200 | 24 | (5)Ol + (50)Cpx + (1)Phl + (44)G |
| 12 | 0.5 | 1150 | 23 | (4)Ol + (66)Cpx + (1)Phl + (29)G |
| *20 wt.% $CaCO_3$ + 1 wt.% $H_2O$* | | | | |
| 10 | 0.5 | 1300 | 15 | (100)G |
| 5 | 0.5 | 1200 | 24 | (3)Ol + (56)Cpx + (1)Phl + (1)Cc + (40)G |
| 7 | 0.5 | 1150 | 24 | (1)Ol + (75)Cpx + (1)Phl + (1)Cc + (22)G |
| *10 wt.% $CaCO_3$ + 5 wt.% $H_2O$* | | | | |
| 24 | 0.5 | 1150 | 11 | (14)Phl + (4)Ol + (20)Cpx + (62)G |
| *10 wt.% $CaMg(CO_3)_2$ + 1 wt.% $H_2O$* | | | | |
| 23 | 0.5 | 1150 | 11 | (15)Ol + (51)Cpx + (1)Phl + (33)G |

Numbers in parenthesis refer to the amount (wt.%) of glass and minerals in each run as estimated by means of mass balance calculations.

Images of experimental products were obtained with a Jeol FE-SEM 6500F equipped with an energy dispersive microanalysis system. Image analysis was performed by using the free WEB software package ImageJ (Image Processing and Analysis in Java; http://rsb.info.nih.gov/ij/).

## 3. Results

### 3.1. Textural features of experimental products

Images of experimental products clearly show significant textural differences between $CaCO_3$-free and $CaCO_3$-bearing experiments (Fig. 1). In particular, the 1200 °C, $CaCO_3$-free run is almost completely glassy, only rare olivine (1 wt.%) is present. On the contrary, $CaCO_3$-bearing runs, at the same temperature, show a high crystal content just after the first 5 wt.% of $CaCO_3$ added; the amount of crystals then increases slowly by adding more carbonate (Table 1). These runs are characterised by the ubiquitous occurrence of clinopyroxene (prevalent), olivine and phlogopite; several poikilitic olivines were also observed (Fig. 2). Notably, runs doped with 20 wt.% of carbonate produced rounded calcite (up to ~10 μm in size), indicative of $CaCO_3$ saturation.

The 1150 °C, $CaCO_3$-free experiment is characterised by the occurrence of rare phlogopite and rhombohedral crystal clusters (<50 μm) made of a central olivine surrounded by clinopyroxenes (Fig. 1). $CaCO_3$-bearing charges are again characterised by the ubiquitous occurrence of clinopyroxene, in larger amount than in the $CaCO_3$-free run (Table 1, Fig. 1), olivine (in several cases poikilitic), phlogopite, and a small amount of glass. The $CaMg(CO_3)_2$-doped run, in agreement with the higher content of magnesium in the starting material, shows the highest olivine content (Table 1).

**Fig. 1.** Backscattered images of $CaCO_3$-free and $CaCO_3$-bearing experimental products. Phase abundances are reported in Table 1. Labels: Ol, olivine; Cpx, clinopyroxene; Phl, phlogopite; Gl: glass; V, vesicles.

Please cite this article as: Mollo, S., et al., Carbonate assimilation in magmas: A reappraisal based on experimental petrology, Lithos (2009), doi:10.1016/j.lithos.2009.10.013

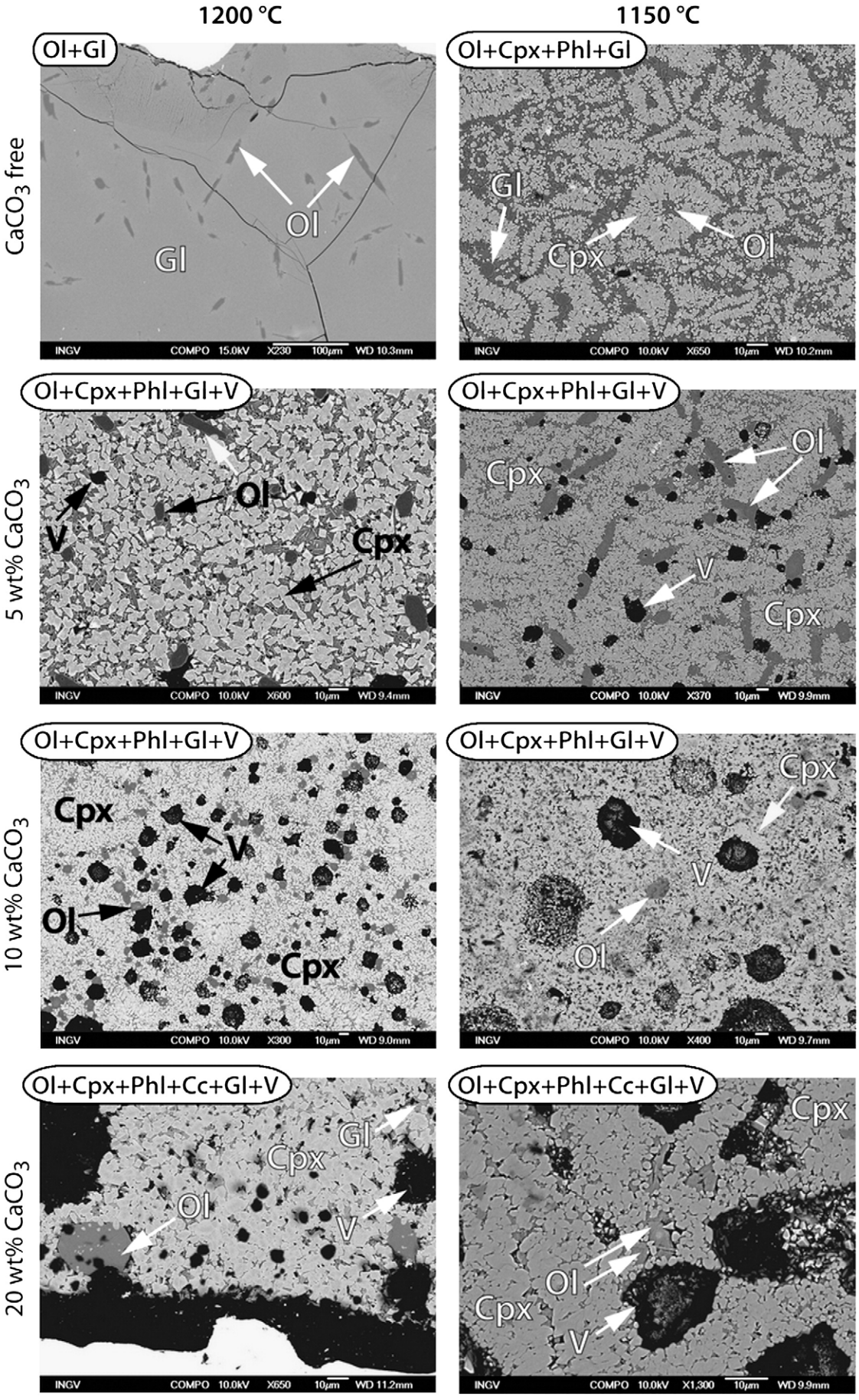


Please cite this article as: Mollo, S., et al., Carbonate assimilation in magmas: A reappraisal based on experimental petrology, Lithos (2009), doi:10.1016/j.lithos.2009.10.013

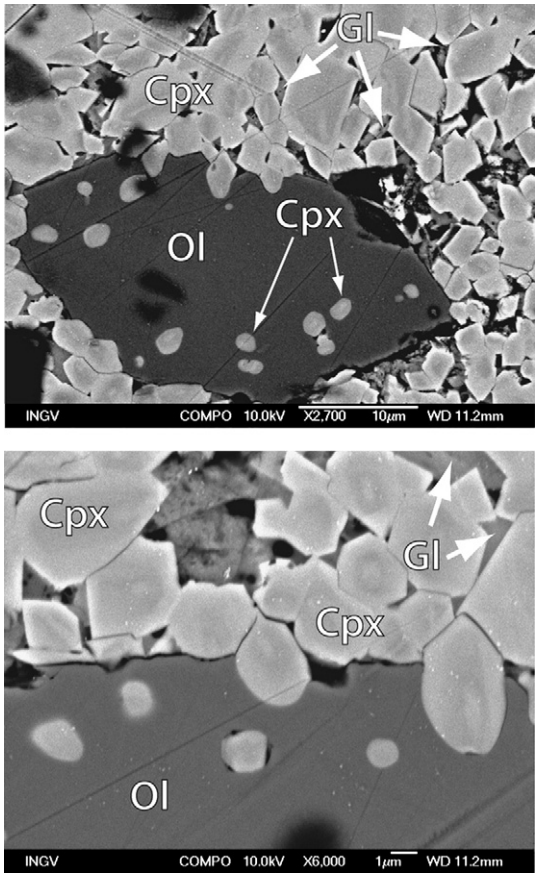


**Fig. 2.** Backscattered images showing clinopyroxenes in poikilitic olivines from the 1200 °C, 20 wt.% $CaCO_3$ run. Labels: Ol, olivine; Cpx, clinopyroxene; Gl: glass.

As general features we observe: i) clinopyroxene crystals remain constant in size in both $CaCO_3$-free and $CaCO_3$-bearing runs (Fig. 1); ii) the number of clinopyroxenes in poikilitic olivines increases as a function of $CaCO_3$; iii) clinopyroxenes are always chemically zoned (Fig. 3); iv) acicular phlogopites occur in very small quantity (about 1 wt.%) in all runs, with the exception of the charge doped with 10 wt.% $CaCO_3$ and 5 wt.% $H_2O$; here phlogopite

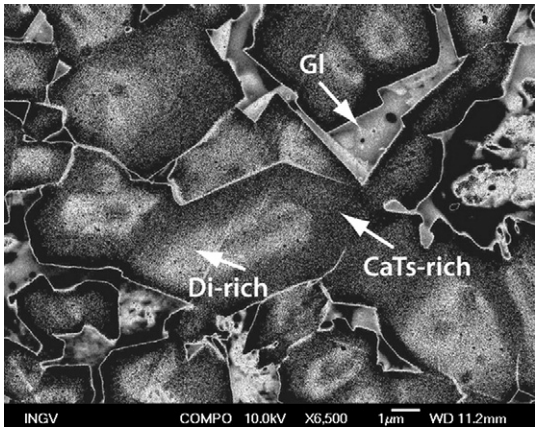


**Fig. 3.** Backscattered image showing core-rim chemical variations of zoned clinopyroxenes. Labels: CaTs, Ca-Tschermak; Di, diopside.

**Table 2**
Representative electron microprobe analyses of experimental olivines. sd represents the standard deviation (in parenthesis number of averaged analyses).

| | *1 wt.% $H_2O$* | | *5 wt.% $CaCO_3$ + 1 wt.% $H_2O$* | | *10 wt.% $CaCO_3$ + 1 wt.% $H_2O$* | | *20 wt.% $CaCO_3$ + 1 wt.% $H_2O$* | | *10 wt.% $CaCO_3$ + 5 wt.% $H_2O$* | | *10 wt.% $CaMg(CO_3)_2$ + 1 wt.% $H_2O$* | |
|---|---|---|---|---|---|---|---|---|---|---|---|---|
| **Run#** | 2 | | 9 | | 6 | | 8 | | 15 | | 12 | | 5 | | 7 | | 24 | | 23 | |
| ***P* (GPa)** | 0.5 | | 0.5 | | 0.5 | | 0.5 | | 0.5 | | 0.5 | | 0.5 | | 0.5 | | 0.5 | | 0.5 | |
| ***T* (°C)** | 1200 | | 1150 | | 1200 | | 1150 | | 1200 | | 1150 | | 1200 | | 1150 | | 1150 | | 1150 | |
| wt.% | | sd(5) | | sd(5) | | sd(5) | | sd(5) | | sd(5) | | sd(5) | | sd(5) | | sd(5) | | sd(5) | | sd(5) |
| $SiO_2$ | 41.95 | 0.26 | 40.67 | 0.29 | 41.51 | 0.54 | 40.50 | 0.11 | 41.22 | 0.36 | 40.60 | 0.35 | 41.00 | 0.14 | 40.66 | 0.20 | 41.97 | 0.34 | 41.35 | 0.54 |
| FeO | 3.74 | 0.69 | 10.39 | 0.67 | 5.81 | 0.18 | 10.70 | 0.35 | 7.89 | 0.94 | 11.72 | 0.43 | 8.43 | 0.17 | 11.85 | 0.40 | 3.00 | 0.12 | 8.50 | 0.67 |
| MgO | 53.82 | 0.76 | 47.84 | 0.41 | 51.95 | 0.40 | 47.55 | 0.97 | 49.95 | 0.51 | 46.80 | 0.77 | 49.34 | 0.08 | 46.38 | 0.13 | 54.55 | 0.40 | 49.52 | 0.32 |
| CaO | 0.40 | 0.06 | 0.58 | 0.29 | 0.58 | 0.17 | 0.70 | 0.03 | 0.79 | 0.18 | 0.86 | 0.17 | 1.09 | 0.05 | 1.10 | 0.17 | 0.45 | 0.06 | 0.59 | 0.29 |
| Total | 99.91 | | 99.49 | | 99.85 | | 99.45 | | 99.85 | | 99.98 | | 99.86 | | 99.99 | | 99.97 | | 99.96 | |
| Formula on the basis of 6 oxygens | | | | | | | | | | | | | | | | | | | | |
| Si | 1.001 | | 1.004 | | 1.000 | | 1.002 | | 1.003 | | 1.004 | | 1.001 | | 1.007 | | 0.789 | | 1.007 | |
| Fe | 0.075 | | 0.215 | | 0.117 | | 0.222 | | 0.161 | | 0.242 | | 0.172 | | 0.245 | | 0.223 | | 0.173 | |
| Mg | 1.914 | | 1.762 | | 1.867 | | 1.755 | | 1.813 | | 1.726 | | 1.797 | | 1.712 | | 2.056 | | 1.798 | |
| Ca | 0.010 | | 0.015 | | 0.015 | | 0.019 | | 0.021 | | 0.023 | | 0.029 | | 0.029 | | 0.142 | | 0.015 | |
| Fo % | 96.25 | | 89.14 | | 93.47 | | 88.79 | | 91.25 | | 87.68 | | 89.14 | | 87.47 | | 97.01 | | 91.22 | |
| Fa % | 3.75 | | 10.86 | | 6.53 | | 11.21 | | 8.75 | | 12.32 | | 10.86 | | 12.53 | | 2.99 | | 8.78 | |

Please cite this article as: Mollo, S., et al., Carbonate assimilation in magmas: A reappraisal based on experimental petrology, Lithos (2009), doi:10.1016/j.lithos.2009.10.013

crystals are sub-euhedral, abundant (about 14 wt.%), and large (up to 1 mm in length); v) rare quench bubbles occur in the interstitial melt of the 1150 °C, $CaCO_3$-free run whereas abundant, larger bubbles occur in all the $CaCO_3$-bearing ones (Fig. 1); vi) sieve-textured rims or skeletal shapes, witnesses of disequilibrium, were not observed.

### 3.2. Experimental phases

Olivine is the liquidus phase only in $CaCO_3$-free experiments. Olivine chemistry varies considerably as a function of experimental conditions. In $CaCO_3$-free experimental products, olivine ranges from $Fo_{96}$ to $Fo_{89}$, at 1200 and 1150 °C, respectively. The highest forsterite content ($Fo_{97}$) was measured in the run doped with 10 wt.% $CaCO_3$ + 5 wt.% $H_2O$; high forsterite content ($Fo_{91}$) was also measured in the $CaMg(CO_3)_2$-doped run (Table 2). In $CaCO_3$-bearing experiments forsterite is generally higher at high temperature and low carbonate content. In particular olivine ranges from $Fo_{93}$ to $Fo_{91}$ with increasing carbonate at 1200 °C and from $Fo_{89}$ to $Fo_{87}$ at 1150 °C. Consistently, CaO increases with increasing the $CaCO_3$ amount loaded in the charges (Fig. 4 and Table 2).

Clinopyroxene crystallizes cotectically with olivine in all $CaCO_3$-bearing runs. Crystals are zoned, the core being more diopsidic than the rim, in both $CaCO_3$-free and $CaCO_3$-bearing runs (Table 3 and Fig. 3). Changes in average clinopyroxene core-to-rim compositions with increasing carbonate in the charge are: i) $Fe^{3+}/Fe^{2+}$ ratio decreases (values calculated according to Putirka et al., 1996); ii) CaO content increases, thus resulting in an increase of CaO-rich pyroxene components (e.g., Ca-Tschermak and hedenbergite; Table 3 and Fig. 5) and in a decrease of CaO-poor components (e.g., enstatite and ferrosilite, Table 3). Diopside and CaFe-Tschermack components remain almost constant (Table 3 and Fig. 5), with the exception of the carbonated water-rich run (10 wt.% $CaCO_3$ + 5 wt.% $H_2O$) where the diopside amount slightly decreases (Table 3) because of phlogopite crystallization (Table 1). Notably, the higher amount of water also favours crystallization of clinopyroxene richer in $Fe^{3+}$ (Table 3).

Phlogopite crystals occur in two populations depending on the amount of water in the charge, the large phlogopite in the carbonated water-rich run shows higher MgO content than phlogopite occurring in $CaCO_3$-bearing runs.

Glass compositions range from tephri-phonolite to foidite as a function of experimental conditions (Fig. 6 and Table 4). Glasses formed in $CaCO_3$-free runs move from the starting K-basalt toward tephri-phonolite while those formed under $CaCO_3$-bearing conditions move towards K-foidite. Notably, experiments doped with 20 wt.% $CaCO_3$ are characterized by the highest degree of crystallization and by $SiO_2$-poor (down to 31 wt.%, not reported in Fig. 6), CaO-rich residual melts (Table 4). Glass in the $CaMg(CO_3)_2$-doped run is less silica undersaturated than the run doped with 10 wt.% $CaCO_3$ (at the same temperature), in agreement with larger olivine crystallisation (Fig. 6). Furthermore, the experiment with 10 wt.% $CaCO_3$ + 5 wt.% $H_2O$, is characterised by Si- and alkali-poor glass due to clinopyroxene and phlogopite crystallization (Fig. 6).

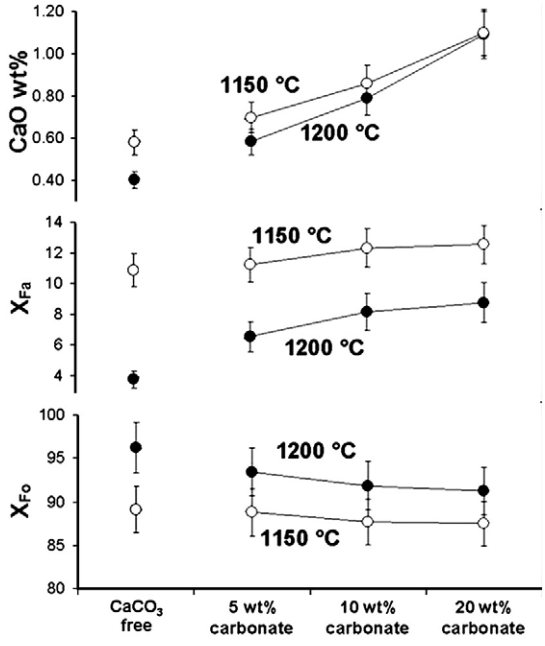


**Fig. 4.** Olivine compositional variations in $CaCO_3$-free and $CaCO_3$-bearing experimental products. Forsterite and fayalite molar fraction ($X_{Fo}$, $X_{Fa}$) and CaO contents in olivine are reported against the amount of $CaCO_3$ in charges.

## 4. Discussion

### 4.1. Texture

Backscattered images of experimental products (Figs. 1, 2, and 3), allow us to reconstruct textural development during the progressive carbonate assimilation.

1. Poikilitic olivines are well developed in $CaCO_3$-bearing runs (Fig. 2) suggesting high clinopyroxene nucleation rate and high olivine growth rate (i.e. $V_{Cpx}^{nucleation} > V_{Ol}^{nucleation}$ and $V_{Ol}^{growth} > V_{Cpx}^{growth}$). In the studied K-basaltic composition, characterised by olivine as the liquidus phase, this texture can be explained by taking into account that carbonate addition favours clinopyroxene nucleation with respect to olivine. Thus, by heating charges up from room temperature (see "Experimental conditions and analytical methods"), the clinopyroxene stability temperature is achieved before the experimental temperature ($T_{Cpx} < T_{exp}$). As a consequence, when the latter is reached, nuclei of clinopyroxene crystals are already present in large amount; an aliquot of these nuclei manage to overstep their equilibrium temperature, surviving as equilibrium phase while an aliquot is partially resorbed during olivine crystallisation (Fig. 2). This texture represents the reverse of the peritectic replacement reaction between olivine and clinopyroxene observed in olivine-bearing cumulate (heteradcumulate) forming at magma–wall rock interface (Gaeta et al., 2009).
2. The number of clinopyroxenes in poikilitic olivines increases with increasing $CaCO_3$ amount in charges, suggesting a positive correlation between $V_{Cpx}^{nucleation}$ and the amount of carbonate.
3. By increasing the amount of carbonate, a significant reduction of melt is observed (Table 1). Interestingly, the texture of the run doped with 20 wt.% of $CaCO_3$, although there is a large amount of clinopyroxenes present, shows chemically homogenous pools and layers of CaO-rich melt among clinopyroxene faces (Table 4, Fig. 2). This therefore agrees with the permeability proposed by Cheadle et al. (2004) and Holness (2005) models. Furthermore, this is also in agreement with the Gaeta et al. (2009) model, suggesting CaO-rich melt migrates from magmatic skarn rocks towards the magma chamber.
4. All $CaCO_3$-bearing runs contain bubbles, demonstrating that carbonate assimilation is a three-phase process (solid, melt, and fluid) characterised by a C–O–H fluid phase.

Please cite this article as: Mollo, S., et al., Carbonate assimilation in magmas: A reappraisal based on experimental petrology, Lithos (2009), doi:10.1016/j.lithos.2009.10.013

**Table 3**
Representative electron microprobe analyses of experimental clinopyroxene. The average value refers to the averaged core–rim composition. sd represents the standard deviation (in parenthesis number of averaged analyses).

| | 1 wt.% $H_2O$ | | | | | 5 wt.% $CaCO_3$ + 1 wt.% $H_2O$ | | | | | | | | | | 10 wt.% $CaCO_3$ + 1 wt.% $H_2O$ | | | | | | |
|---|---|---|---|---|---|---|---|---|---|---|---|---|---|---|---|---|---|---|---|---|---|---|
| **Run#** | 9 | | | | | 6 | | | | | 8 | | | | | 15 | | | | | 12 | |
| ***P*** | | | | | | | | | | | | | | | | | | | | | | |
| **(GPa)** | 0.5 | | | | | 0.5 | | | | | 0.5 | | | | | 0.5 | | | | | 0.5 | |
| ***T* (°C)** | 1150 | | | | | 1200 | | | | | 1150 | | | | | 1200 | | | | | 1150 | |
| wt.% | Core | sd (5) | Rim | sd (5) | Average | Core | sd (5) | Rim | sd (5) | Average | Core | sd (5) | Rim | sd (5) | Average | Core | sd (5) | Rim | sd (5) | Average | Core | sd (5) |
| $SiO_2$ | 48.60 | 0.21 | 48.40 | 0.23 | 48.50 | 48.72 | 0.44 | 48.58 | 0.23 | 48.65 | 48.22 | 0.34 | 48.14 | 0.30 | 48.18 | 48.50 | 0.26 | 48.21 | 0.22 | 48.36 | 48.00 | 0.32 |
| $TiO_2$ | 0.78 | 0.02 | 0.79 | 0.03 | 0.79 | 0.70 | 0.03 | 0.71 | 0.03 | 0.71 | 0.70 | 0.06 | 0.73 | 0.05 | 0.72 | 0.66 | 0.02 | 0.68 | 0.02 | 0.67 | 0.66 | 0.05 |
| $Al_2O_3$ | 5.83 | 0.23 | 6.09 | 0.26 | 5.96 | 8.00 | 0.35 | 8.20 | 0.29 | 8.10 | 8.45 | 0.37 | 8.78 | 0.30 | 8.62 | 8.55 | 0.35 | 8.65 | 0.35 | 8.60 | 8.83 | 0.26 |
| FeO | 6.39 | 0.32 | 6.80 | 0.26 | 6.60 | 4.00 | 0.40 | 4.18 | 0.31 | 4.09 | 4.27 | 0.38 | 4.80 | 0.30 | 4.54 | 3.95 | 0.44 | 4.50 | 0.33 | 4.23 | 4.40 | 0.37 |
| MgO | 14.77 | 0.16 | 14.10 | 0.16 | 14.44 | 14.96 | 0.29 | 14.57 | 0.21 | 14.77 | 14.40 | 0.33 | 13.45 | 0.27 | 13.93 | 14.40 | 0.32 | 13.68 | 0.29 | 14.04 | 13.90 | 0.23 |
| CaO | 23.00 | 0.25 | 23.15 | 0.22 | 23.08 | 23.09 | 0.19 | 23.20 | 0.25 | 23.15 | 23.34 | 0.19 | 23.49 | 0.11 | 23.42 | 23.40 | 0.27 | 23.69 | 0.26 | 23.55 | 23.60 | 0.24 |
| $Na_2O$ | 0.15 | 0.02 | 0.17 | 0.02 | 0.16 | 0.20 | 0.02 | 0.21 | 0.02 | 0.21 | 0.20 | 0.03 | 0.24 | 0.02 | 0.22 | 0.23 | 0.03 | 0.24 | 0.01 | 0.24 | 0.22 | 0.03 |
| $K_2O$ | 0.04 | 0.02 | 0.06 | 0.03 | 0.05 | 0.07 | 0.02 | 0.07 | 0.01 | 0.07 | 0.07 | 0.03 | 0.08 | 0.02 | 0.08 | 0.10 | 0.01 | 0.10 | 0.03 | 0.10 | 0.09 | 0.02 |
| Total | 99.56 | | 99.56 | | 99.56 | 99.74 | | 99.72 | | 99.73 | 99.65 | | 99.71 | | 99.68 | 99.79 | | 99.75 | | 99.77 | 99.70 | |
| Formula on the basis of 6 oxygens | | | | | | | | | | | | | | | | | | | | | | |
| Si | 1.793 | | 1.791 | | 1.792 | 1.779 | | 1.777 | | 1.778 | 1.766 | | 1.769 | | 1.768 | 1.772 | | 1.768 | | 1.770 | 1.759 | |
| Ti | 0.022 | | 0.022 | | 0.022 | 0.019 | | 0.020 | | 0.019 | 0.019 | | 0.020 | | 0.020 | 0.018 | | 0.019 | | 0.018 | 0.018 | |
| $Al^{IV}$ | 0.207 | | 0.209 | | 0.208 | 0.221 | | 0.223 | | 0.222 | 0.234 | | 0.231 | | 0.232 | 0.228 | | 0.232 | | 0.230 | 0.241 | |
| $Al^{VI}$ | 0.047 | | 0.057 | | 0.052 | 0.124 | | 0.131 | | 0.127 | 0.131 | | 0.150 | | 0.140 | 0.140 | | 0.142 | | 0.141 | 0.141 | |
| $Fe^{3+}$ | 0.129 | | 0.123 | | 0.126 | 0.076 | | 0.071 | | 0.074 | 0.082 | | 0.062 | | 0.072 | 0.073 | | 0.073 | | 0.073 | 0.083 | |
| $Fe^{2+}$ | 0.068 | | 0.087 | | 0.078 | 0.046 | | 0.057 | | 0.051 | 0.048 | | 0.086 | | 0.067 | 0.048 | | 0.065 | | 0.056 | 0.052 | |
| Mg | 0.812 | | 0.778 | | 0.795 | 0.814 | | 0.794 | | 0.804 | 0.786 | | 0.737 | | 0.761 | 0.784 | | 0.748 | | 0.766 | 0.759 | |
| Ca | 0.909 | | 0.918 | | 0.914 | 0.903 | | 0.909 | | 0.906 | 0.916 | | 0.925 | | 0.920 | 0.916 | | 0.931 | | 0.924 | 0.927 | |
| Na | 0.011 | | 0.012 | | 0.011 | 0.014 | | 0.015 | | 0.015 | 0.014 | | 0.017 | | 0.016 | 0.016 | | 0.017 | | 0.017 | 0.016 | |
| K | 0.002 | | 0.003 | | 0.002 | 0.003 | | 0.003 | | 0.003 | 0.003 | | 0.004 | | 0.004 | 0.005 | | 0.005 | | 0.005 | 0.004 | |
| Di | 0.668 | | 0.657 | | 0.663 | 0.664 | | 0.659 | | 0.662 | 0.660 | | 0.640 | | 0.650 | 0.665 | | 0.661 | | 0.663 | 0.660 | |
| Hd | 0.056 | | 0.074 | | 0.065 | 0.037 | | 0.047 | | 0.042 | 0.041 | | 0.075 | | 0.057 | 0.041 | | 0.057 | | 0.049 | 0.045 | |
| En | 0.072 | | 0.060 | | 0.066 | 0.075 | | 0.068 | | 0.071 | 0.063 | | 0.048 | | 0.055 | 0.059 | | 0.043 | | 0.051 | 0.050 | |
| Fs | 0.006 | | 0.007 | | 0.006 | 0.004 | | 0.005 | | 0.005 | 0.004 | | 0.006 | | 0.005 | 0.004 | | 0.004 | | 0.004 | 0.003 | |
| CaTs | 0.099 | | 0.103 | | 0.101 | 0.144 | | 0.148 | | 0.146 | 0.154 | | 0.160 | | 0.157 | 0.156 | | 0.157 | | 0.156 | 0.163 | |
| CaFeTs | 0.065 | | 0.062 | | 0.063 | 0.038 | | 0.036 | | 0.037 | 0.041 | | 0.031 | | 0.036 | 0.036 | | 0.037 | | 0.036 | 0.042 | |
| CaTiTs | 0.022 | | 0.022 | | 0.022 | 0.019 | | 0.020 | | 0.019 | 0.019 | | 0.020 | | 0.020 | 0.018 | | 0.019 | | 0.018 | 0.018 | |

### 4.2. Redox state

$CaCO_3$-free experiments were carried out under O–H fluid-absent conditions and their redox state was computed according to the Kress and Carmichael (1991) equation, using $Fe^{2+}$ content of the melt estimated from the $^{Ol\text{-}melt}Kd_{Fe-Mg} = 0.3 \pm 0.03$ (Roeder and Emslie, 1970) and $^{Cpx\text{-}melt}Kd_{Fe-Mg} = 0.27 \pm 0.03$ (Putirka, 1999). The calculated $fO_2$ value of NNO + 1.5 (±0.2) is consistent with the intrinsic buffer of the piston cylinder apparatus (Kushiro, 1990; Kawamoto and Hirose, 1994; Freda et al., 2008).

$CaCO_3$-bearing experiments were carried out under C–O–H fluid-present conditions, as testified by the occurrence of bubbles increasing in size from micrometric to millimetric by increasing the amount of $CaCO_3$ in charges. Carbonate dissolution, by introducing $CO_2$ in the system, drops water solubility in the melt phase, induces a progressive increase of $CO_2/H_2O$ ratio in the free-fluid phase, and promotes bubble growth. Under these conditions, the $fO_2$ value is lowered by about two log units (Kadik et al., 2004; Botcharnikov et al., 2005a,b; Schuessler et al., 2008; Behrens et al., 2009), and is consistent with the negative correlation between Fa in olivine and $Fe^{3+}/Fe^{2+}$ ratio in clinopyroxene as a function of the addition of $CaCO_3$ (Figs. 4 and 5). However, this is not in conflict with the suggestion of Wenzel et al. (2002) that natural systems are affected by a $fO_2$ increase during magma–carbonate interaction. In open natural systems, volatiles are free to escape (Barnes et al., 2005), therefore $CO_2$ effect on $fO_2$ may be less. Actually, magmatic skarns are characterised by clinopyroxenes and Al-spinels showing wide variability in the $Fe^{3+}/Fe^{2+}$ ratio (Gaeta et al., 2009), suggesting $fO_2$ fluctuation during carbonate assimilation.

### 4.3. Mg–$Fe^{2+}$ partitioning between olivine and melt

Theoretical and experimental studies have demonstrated that $^{Ol\text{-}melt}Kd_{Fe-Mg}$ is sensitive to temperature, pressure, and melt composition (e.g., Longhi et al., 1978, Sack et al., 1987; Gee and Sack, 1988; Kushiro and Walter, 1998; Kushiro and Mysen, 2002; Toplis, 2005). With the aim of determining the main factor controlling Mg–$Fe^{2+}$ partitioning between olivine and melt during the progressive carbonate assimilation, we calculated $^{Ol\text{-}melt}Kd_{Fe-Mg}$ of $CaCO_3$-bearing experiments. $Fe^{2+}/Fe^{3+}$ partitioning in the melt was estimated by considering that under C–O–H fluid-present conditions, the $fO_2$ is lowered by about two log units with respect to the intrinsic buffer (NNO + 1.5) of the experimental apparatus (Kadik et al., 2004; Botcharnikov et al., 2005a,b; Schuessler et al., 2008; Behrens et al., 2009). The values obtained of $^{Ol\text{-}melt}Kd_{Fe-Mg}$ range from 0.27 to 0.33 at 1200 °C and from 0.28 to 0.63 al 1150 °C. As all the experiments were performed at 0.5 GPa and in a relatively narrow temperature range, such a large variation of the $^{Ol\text{-}melt}Kd_{Fe-Mg}$ is likely to be related to melt compositional variation induced by carbonate assimilation (Fig. 7). In particular, Fig. 7a and b shows that melt $SiO_2$ decreases and depolymerization increases, produced by the ongoing carbonate assimilation, are positively correlated with $^{Ol\text{-}melt}Kd_{Fe-Mg}$ values. This feature is in agreement with the observation that melt silica content is the major factor controlling Mg–$Fe^{2+}$ partitioning between olivine and the melt (Longhi et al., 1978; O'Neill and Eggins, 2002; Toplis, 2005) and that $^{Ol\text{-}melt}Kd_{Fe-Mg}$ increases with the increase of the Non-Bridging Oxygen/Tetrahedra ratio (up to NBO/T = 2, Kushiro and Mysen, 2002). Notably, for these compositions, the negative correlation between alkalis and $^{Ol\text{-}melt}Kd_{Fe-Mg}$ (cf., Gee and Sack, 1988;

Please cite this article as: Mollo, S., et al., Carbonate assimilation in magmas: A reappraisal based on experimental petrology, Lithos (2009), doi:10.1016/j.lithos.2009.10.013

| | | | 20 wt.% $CaCO_3$ + 1 wt.% $H_2O$ | | | | | | | | | | 10 wt.% $CaCO_3$ + 5 wt.% $H_2O$ | | | | | 10 wt.% $CaMg(CO_3)_2$ + 1 wt.% $H_2O$ | | | | |
|---|---|---|---|---|---|---|---|---|---|---|---|---|---|---|---|---|---|---|---|---|---|---|
| | | | 5 | | | | | 7 | | | | | 15 | | | | | 24 | | | | |
| | | | 0.5 | | | | | 0.5 | | | | | 0.5 | | | | | 0.5 | | | | |
| | | | 1200 | | | | | 1150 | | | | | 1150 | | | | | 1150 | | | | |
| Rim | sd (5) | Average | Core | sd (5) | Rim | sd (5) | Average | Core | sd (5) | Rim | sd (5) | Average | Core | sd (5) | Rim | sd (5) | Average | Core | sd (5) | Rim | sd (5) | Average |
| 47.91 | 0.26 | 47.96 | 47.93 | 0.32 | 47.48 | 0.36 | 47.71 | 47.55 | 0.35 | 47.41 | 0.34 | 47.48 | 46.00 | 0.34 | 45.60 | 0.32 | 45.80 | 48.60 | 0.37 | 48.50 | 0.30 | 48.55 |
| 0.68 | 0.05 | 0.67 | 0.56 | 0.04 | 0.60 | 0.01 | 0.58 | 0.56 | 0.06 | 0.60 | 0.12 | 0.58 | 0.77 | 0.05 | 0.80 | 0.06 | 0.78 | 0.50 | 0.14 | 0.50 | 0.15 | 0.50 |
| 9.17 | 0.36 | 9.00 | 9.25 | 0.31 | 9.44 | 0.32 | 9.35 | 9.35 | 0.28 | 9.69 | 0.33 | 9.52 | 9.09 | 0.30 | 9.35 | 0.29 | 9.22 | 7.70 | 0.29 | 8.02 | 0.32 | 7.86 |
| 4.88 | 0.28 | 4.64 | 4.15 | 0.29 | 4.95 | 0.32 | 4.55 | 4.78 | 0.31 | 5.22 | 0.37 | 5.00 | 6.20 | 0.25 | 6.78 | 0.28 | 6.49 | 4.70 | 0.31 | 5.10 | 0.33 | 4.90 |
| 13.01 | 0.27 | 13.46 | 13.38 | 0.26 | 12.67 | 0.24 | 13.03 | 12.95 | 0.27 | 12.07 | 0.33 | 12.51 | 13.55 | 0.28 | 12.85 | 0.29 | 13.20 | 14.50 | 0.27 | 13.75 | 0.31 | 14.13 |
| 23.79 | 0.16 | 23.70 | 24.10 | 0.14 | 24.20 | 0.15 | 24.15 | 24.13 | 0.14 | 24.40 | 0.24 | 24.27 | 23.40 | 0.13 | 23.60 | 0.14 | 23.50 | 23.34 | 0.21 | 23.55 | 0.24 | 23.45 |
| 0.22 | 0.04 | 0.22 | 0.23 | 0.02 | 0.22 | 0.02 | 0.23 | 0.23 | 0.04 | 0.21 | 0.04 | 0.22 | 0.24 | 0.02 | 0.25 | 0.02 | 0.25 | 0.19 | 0.05 | 0.19 | 0.03 | 0.19 |
| 0.10 | 0.03 | 0.10 | 0.10 | 0.03 | 0.11 | 0.02 | 0.11 | 0.11 | 0.02 | 0.11 | 0.03 | 0.11 | 0.07 | 0.01 | 0.08 | 0.01 | 0.08 | 0.09 | 0.02 | 0.09 | 0.03 | 0.09 |
| 99.76 | | 99.73 | 99.70 | | 99.67 | | 99.69 | 99.66 | | 99.71 | | 99.69 | 99.32 | | 99.31 | | 99.32 | 99.62 | | 99.70 | | 99.66 |
| 1.762 | | 1.761 | 1.758 | | 1.749 | | 1.754 | 1.749 | | 1.751 | | 1.750 | 1.699 | | 1.690 | | 1.695 | 1.782 | | 1.783 | | 1.783 |
| 0.019 | | 0.019 | 0.015 | | 0.017 | | 0.016 | 0.015 | | 0.017 | | 0.016 | 0.021 | | 0.022 | | 0.022 | 0.014 | | 0.014 | | 0.014 |
| 0.238 | | 0.239 | 0.242 | | 0.251 | | 0.246 | 0.251 | | 0.249 | | 0.250 | 0.301 | | 0.310 | | 0.305 | 0.218 | | 0.217 | | 0.217 |
| 0.160 | | 0.150 | 0.158 | | 0.159 | | 0.158 | 0.155 | | 0.172 | | 0.164 | 0.095 | | 0.099 | | 0.097 | 0.115 | | 0.131 | | 0.123 |
| 0.061 | | 0.072 | 0.074 | | 0.079 | | 0.077 | 0.087 | | 0.064 | | 0.075 | 0.184 | | 0.188 | | 0.186 | 0.093 | | 0.077 | | 0.085 |
| 0.089 | | 0.071 | 0.053 | | 0.073 | | 0.063 | 0.060 | | 0.097 | | 0.079 | 0.007 | | 0.022 | | 0.015 | 0.051 | | 0.080 | | 0.065 |
| 0.713 | | 0.736 | 0.731 | | 0.696 | | 0.714 | 0.710 | | 0.664 | | 0.687 | 0.746 | | 0.710 | | 0.728 | 0.792 | | 0.753 | | 0.773 |
| 0.938 | | 0.932 | 0.947 | | 0.955 | | 0.951 | 0.951 | | 0.965 | | 0.958 | 0.926 | | 0.937 | | 0.932 | 0.917 | | 0.928 | | 0.922 |
| 0.016 | | 0.016 | 0.016 | | 0.016 | | 0.016 | 0.016 | | 0.015 | | 0.016 | 0.017 | | 0.018 | | 0.018 | 0.014 | | 0.014 | | 0.014 |
| 0.005 | | 0.004 | 0.005 | | 0.005 | | 0.005 | 0.005 | | 0.005 | | 0.005 | 0.003 | | 0.004 | | 0.004 | 0.004 | | 0.004 | | 0.004 |
| 0.639 | | 0.649 | 0.672 | | 0.652 | | 0.662 | 0.660 | | 0.639 | | 0.650 | 0.640 | | 0.630 | | 0.635 | 0.670 | | 0.655 | | 0.655 |
| 0.080 | | 0.062 | 0.049 | | 0.069 | | 0.058 | 0.056 | | 0.094 | | 0.075 | 0.006 | | 0.019 | | 0.013 | 0.043 | | 0.070 | | 0.070 |
| 0.037 | | 0.043 | 0.030 | | 0.022 | | 0.026 | 0.025 | | 0.013 | | 0.019 | 0.053 | | 0.040 | | 0.046 | 0.061 | | 0.049 | | 0.049 |
| 0.005 | | 0.004 | 0.002 | | 0.002 | | 0.002 | 0.002 | | 0.002 | | 0.002 | 0.001 | | 0.001 | | 0.001 | 0.004 | | 0.005 | | 0.005 |
| 0.170 | | 0.166 | 0.174 | | 0.178 | | 0.176 | 0.176 | | 0.184 | | 0.180 | 0.166 | | 0.171 | | 0.169 | 0.144 | | 0.151 | | 0.151 |
| 0.030 | | 0.036 | 0.037 | | 0.040 | | 0.038 | 0.043 | | 0.032 | | 0.038 | 0.092 | | 0.094 | | 0.093 | 0.047 | | 0.038 | | 0.038 |
| 0.019 | | 0.019 | 0.015 | | 0.017 | | 0.016 | 0.015 | | 0.017 | | 0.016 | 0.021 | | 0.022 | | 0.022 | 0.014 | | 0.014 | | 0.014 |

Carmichael and Ghiorso, 1990; Falloon et al., 1997; Sugawara, 1998; Toplis, 2005) is not evident (Fig. 7c).

### 4.4. Carbonate assimilation reaction

The dissolution reaction of $CaCO_3$ in silicate melts producing silica-undersaturated hybrid melt compositions was schematised as follow (cf., Iacono Marziano et al., 2008):

$$CaCO_3^{solid} + SiO_2^{melt} + MgO^{melt} \rightarrow Diopside^{solid} + CO_2^{fluid} \quad (1)$$

According to this reaction, carbonate incorporation into silicate melt leads toward silica-undersaturated melts by consuming $SiO_2$ to form diopside; this implies that the extent of carbonate assimilation is controlled by the MgO content in the melt. Although this reaction may apply to primitive basaltic magma, it is surely not suitable to describe assimilation occurring in intermediate and evolved magma systems (Barnes et al., 2005; Freda et al., 2008).

Experimental results from this study show that in a $CaCO_3$-bearing system, Ca-Tschermak and hedenbergite components increase as a function of $CaCO_3$ addition, whereas diopside molar fraction remains almost constant (Fig. 5). In light of this, the desilication reaction that yields silica-undersaturated melts (Fig. 6), is driven by the crystallization of a Mg-, Al-, Fe-clinopyroxene solid solution rather than by a diopside *sensu stricto*.

This process is shown in Fig. 8 where Ca-Tschermak (CaTs), hedenbergite (Hd), and diopside (Di) contents of clinopyroxenes from experiments performed at 1200 and 1150 °C and variable $CaCO_3$ contents, are plotted versus their respective molar fractions ($X_{CaTs}$, $X_{Hd}$, $X_{Di}$). Fig. 8a and b shows that mass and molar fraction of CaTs and Hd increase as a function of both $CaCO_3$ addition and decreasing temperature; as a consequence, assimilation and fractional crystallisation vectors coincide. On the other hand, diopside molar fraction remains almost constant during increase in $CaCO_3$ amount, while its wt.% increases as a function of decreasing temperature; therefore, assimilation and fractional crystallisation vectors follow different directions (Fig. 8c).

Unlike reaction (1), our experiments highlight that carbonate assimilation has an effect not only on Di, but also on CaTs and Hd clinopyroxene components. We thus propose that the carbonate assimilation reaction should be re-written as:

$$CaCO_3^{solid} + SiO_2^{melt} + MgO^{melt} + FeO^{melt} + Al_2O_3^{melt} \rightarrow (Di - Hd - CaTs)_{ss}^{solid} + CO_2^{fluid} \quad (2)$$

This reaction describes the carbonate assimilation process leading to the formation of magmatic skarns. These rocks are characterised by CaTs-rich clinopyroxene showing chemical compositions comparable with clinopyroxenes occurring in $CaCO_3$-bearing experimental products (Table 5 and Fig. 9). Moreover, magmatic skarns are characterised by interstitial glasses showing a $SiO_2$-poor, CaO-rich composition

Please cite this article as: Mollo, S., et al., Carbonate assimilation in magmas: A reappraisal based on experimental petrology, Lithos (2009), doi:10.1016/j.lithos.2009.10.013

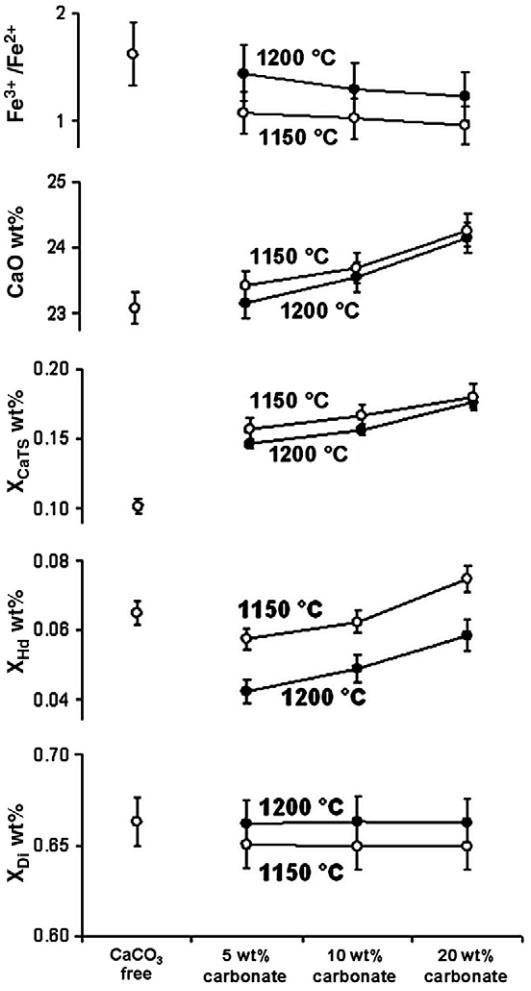


**Fig. 5.** Clinopyroxene compositional variations in $CaCO_3$-free and $CaCO_3$-bearing experimental products. Diopside, hedenbergite, Ca-Tschermak molar fraction ($X_{Di}$, $X_{Hd}$, $X_{CaTs}$), CaO content, and $Fe^{3+}/Fe^{2+}$ in clinopyroxene are reported against the amount of $CaCO_3$ in charges.

(Table 5) similar to the glass composition obtained in runs doped with 20 wt.% $CaCO_3$ (Table 4 and Fig. 6).

### 4.5. Thermo-barometric application to skarn rocks

The Colli Albani Volcanic District, belonging to the ultrapotassic Roman Province (Peccerillo, 2005), represents one of the best examples of plumbing system emplaced in thick carbonate substrata (Freda et al., 2008 and references therein). Recent papers (Dallai et al., 2004; Gaeta et al., 2006; Freda et al., 2008) have demonstrated that the extraordinary chemistry (low $SiO_2$ values, high $K_2O$ and CaO contents, and generally low Mg-number) of K-foiditic rocks outcropping at Colli Albani, results from the interaction between magma and carbonate wall-rocks.

The important role played by carbonate assimilation during the Colli Albani magmatism is also attested by the presence of magmatic skarn xenoliths characterized by Ca-Tschermak-rich clinopyroxenes (Fig. 9 and Table 5). According to Gaeta et al. (2009) these rocks formed after carbonate contamination of potassic magma at relatively low pressure (lower than 0.3 GPa) and high temperature (1100–1200 °C). Thermo-barometric conditions for their formation were deduced from melt inclusions in olivines from cumulate rocks associated with skarns and from the occurrence of glass in the skarn rocks themselves. Unfortunately, no direct thermo-barometric calculations on Colli Albani skarn phases, or on similar rocks occurring in other volcanic districts emplaced in carbonate substrate (e.g. Vesuvius), are available.

Solid state reactions generally used as thermo-barometers for thermo-metamorphic carbonate rocks, cannot be applied to the magmatic skarns characterised by modal clinopyroxene and silicate glass; moreover, the reliability of thermo-barometric equations has never been proved for carbonated silicate-melts. In order to verify their applicability, we tested the most suitable thermo-barometric equations against clinopyroxene–liquid equilibria on melt and clinopyroxene chemistries experimentally obtained in this study. We applied the Nimis (1995), Putirka

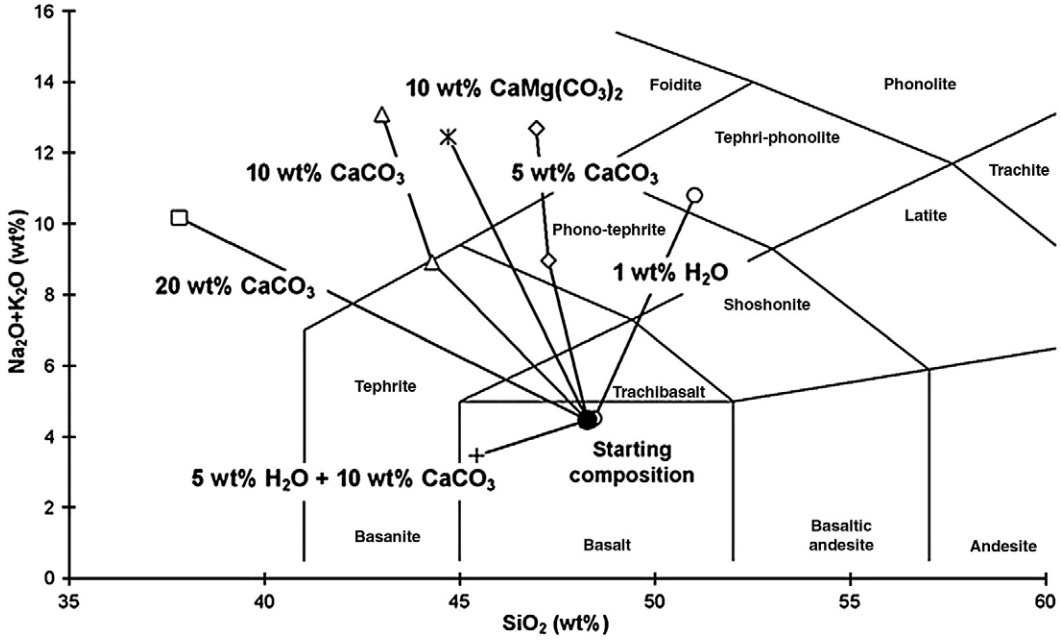


**Fig. 6.** TAS diagram showing composition of experimental residual glasses.

Please cite this article as: Mollo, S., et al., Carbonate assimilation in magmas: A reappraisal based on experimental petrology, Lithos (2009), doi:10.1016/j.lithos.2009.10.013

**Table 4**
Representative electron microprobe analyses of experimental glasses (normalised).

| | 1 wt.% $H_2O$ | | | | 5 wt.% $CaCO_3$ + 1 wt.% $H_2O$ | | | | 10 wt.% $CaCO_3$ + 1 wt.% $H_2O$ | | | | | | | |
|---|---|---|---|---|---|---|---|---|---|---|---|---|---|---|---|---|
| Run# | 2 | | 9 | | 14 | | 6 | | 8 | | 13 | | 15 | | 12 | |
| *P* (GPa) | 0.5 | | 0.5 | | 0.5 | | 0.5 | | 0.5 | | 0.5 | | 0.5 | | 0.5 | |
| *T* (°C) | 1200 | | 1150 | | 1300 | | 1200 | | 1150 | | 1300 | | 1200 | | 1150 | |
| wt.% | | sd(5) | | sd(5) | | sd(5) | | sd(5) | | sd(5) | | sd(5) | | sd(5) | | sd(5) |
| $SiO_2$ | 48.45 | 0.62 | 51.02 | 1.09 | 46.83 | 0.45 | 47.27 | 1.13 | 46.95 | 1.07 | 45.71 | 0.99 | 44.28 | 1.02 | 43.00 | 1.20 |
| $TiO_2$ | 0.71 | 0.03 | 0.70 | 0.01 | 0.68 | 0.03 | 0.76 | 0.01 | 0.67 | 0.13 | 0.65 | 0.03 | 0.69 | 0.02 | 0.76 | 0.07 |
| $Al_2O_3$ | 11.52 | 0.21 | 19.00 | 0.72 | 11.02 | 0.66 | 14.71 | 0.89 | 19.98 | 0.77 | 10.85 | 0.79 | 14.00 | 0.90 | 16.04 | 0.82 |
| FeO | 7.40 | 0.13 | 7.40 | 0.33 | 6.65 | 0.29 | 7.10 | 0.29 | 7.20 | 0.34 | 6.13 | 0.10 | 7.00 | 0.33 | 7.10 | 0.49 |
| MgO | 13.26 | 0.30 | 3.98 | 0.49 | 14.00 | 0.39 | 7.20 | 0.63 | 5.30 | 0.64 | 12.10 | 0.31 | 6.40 | 0.55 | 4.90 | 0.50 |
| CaO | 14.15 | 0.71 | 7.10 | 0.68 | 16.47 | 0.29 | 14.00 | 0.31 | 7.20 | 0.41 | 20.47 | 0.24 | 18.71 | 0.29 | 15.11 | 0.30 |
| $Na_2O$ | 1.22 | 0.06 | 3.00 | 0.33 | 1.17 | 0.10 | 2.57 | 0.21 | 3.06 | 0.30 | 1.12 | 0.09 | 2.32 | 0.40 | 3.46 | 0.10 |
| $K_2O$ | 3.29 | 0.07 | 7.80 | 0.43 | 3.17 | 0.14 | 6.38 | 0.52 | 9.64 | 0.27 | 2.97 | 0.23 | 6.60 | 0.42 | 9.64 | 0.20 |
| Total | 100.00 | | 100.00 | | 100.00 | | 100.00 | | 100.00 | | 100.00 | | 100.00 | | 100.00 | |
| Total[a] | 98.91 | | 98.01 | | 98.59 | | 97.83 | | 97.12 | | 97.92 | | 97.07 | | 96.33 | |

| | 20 wt.% $CaCO_3$ + 1 wt.% $H_2O$ | | | | | | 10 wt.% $CaCO_3$ + 5 wt.% $H_2O$ | | 10 wt.% $CaMg(CO_3)_2$ + 1 wt.% $H_2O$ | |
|---|---|---|---|---|---|---|---|---|---|---|
| Run# | 10 | | 5 | | 7 | | 24 | | 23 | |
| *P* (GPa) | 0.5 | | 0.5 | | 0.5 | | 0.5 | | 0.5 | |
| *T* (°C) | 1300 | | 1200 | | 1150 | | 1150 | | 1150 | |
| wt.% | | sd(5) | | sd(5) | | sd(5) | | sd(5) | | sd(5) |
| $SiO_2$ | 43.53 | 1.01 | 37.82 | 1.17 | 31.00 | 1.05 | 45.42 | 1.25 | 44.69 | 1.00 |
| $TiO_2$ | 0.61 | 0.02 | 0.67 | 0.02 | 0.81 | 0.02 | 0.54 | 0.03 | 0.71 | 0.02 |
| $Al_2O_3$ | 10.08 | 0.81 | 14.05 | 0.78 | 12.16 | 0.93 | 14.57 | 0.87 | 18.05 | 0.78 |
| FeO | 6.00 | 0.28 | 7.00 | 0.35 | 8.10 | 0.41 | 6.15 | 0.31 | 8.00 | 0.16 |
| MgO | 11.35 | 0.32 | 5.40 | 0.44 | 5.70 | 0.49 | 6.50 | 0.51 | 6.10 | 0.34 |
| CaO | 24.50 | 0.31 | 24.90 | 0.36 | 26.83 | 0.40 | 23.35 | 0.45 | 10.00 | 0.31 |
| $Na_2O$ | 1.06 | 0.10 | 2.88 | 0.16 | 3.80 | 0.25 | 1.75 | 0.20 | 3.30 | 0.17 |
| $K_2O$ | 2.86 | 0.24 | 7.28 | 0.28 | 11.60 | 0.38 | 1.71 | 0.30 | 9.15 | 0.29 |
| Total | 100.00 | | 100.00 | | 100.00 | | 100.00 | | 100.00 | |
| Total[a] | 97.37 | | 95.93 | | 93.74 | | 92.97 | | 97.08 | |

sd represents the standard deviation (in parenthesis number of averaged analyses).
[a] WDS-EMP total.

et al. (1996), Nimis and Ulmer (1998), Putirka et al. (2003), and Putirka (2008) thermo-barometric equations to 72 clinopyroxene–melt couples from $CaCO_3$-bearing runs. Each model produced a range of possible temperature and pressure. Then, we calculated the standard error of estimate (SEE) for pressure and temperature with respect to our experimental conditions (Table 6). According to the obtained SEE values, the best predictive equations are 32a, 32b (Putirka, 2008) and T1 (Putirka et al., 1996) for pressure, and 34 (Putirka, 2008) for temperature. All the considered equations give SEE below 10% of the experimental temperatures and thus all can be considered suitable. In contrast, for pressure prediction some of the used models give SEE up to 100% of the experimental value of 0.5 GPa. Interestingly, the most suitable equations are those based upon clinopyroxene "alone" composition while the only equation based on clinopyroxene–melt equilibrium giving a low systematic error is the P1 equation of Putirka et al. (1996) which was designed for anhydrous systems. By applying equations 32a and T1 to estimate pressure and temperature crystallization conditions of glass-bearing magmatic skarns from Colli Albani, we obtain (Table 5) pressure values ranging from 0.25 to 0.32 GPa and temperatures in the range 1081–1126 °C. These values are in good agreement with crystallization conditions ($P = 0.2$–$0.3$ GPa and $T = 1180$ °C) estimated by Gaeta et al. (2009) for olivine-bearing cumulates associated with magmatic skarns. However, we speculate that equations designed for hydrous systems are not suitable for carbonated melts because of the well-known $CO_2$ effect on water activity (e.g. Behrens et al., 2009). Therefore, barometric equations based on mineral-liquid equilibria, in order to be applied to carbonated systems, must be designed taking into account that carbonate assimilation is a process involving three-phases, solid, melt and fluid (C–O–H).

## 5. Conclusions

Experimental results from this study demonstrate that the carbonate assimilation reaction is more complex than so far assumed. Carbonate assimilation is a three-phase (solid, melt, and fluid) process whose main products are: diopside-hedenbergite-Ca-Tschermak clinopyroxene solid solution, silica-undersaturated CaO-rich melt, and C–O–H fluid phase. Magma–carbonate interaction affects texture, phase chemistry, redox state, and equilibrium condition of experimental carbonated systems as follow: i) $V_{Cpx}^{nucleation} > V_{Ol}^{nucleation}$ and $V_{Ol}^{growth} > V_{Cpx}^{growth}$; ii) Ca-Tschermak and hedenbergite components in clinopyroxene are favoured; iii) silica decrease (high NBO/T) has a significant effect on the Mg–$Fe^{2+}$ partitioning between olivine and melt; iv) Fa in olivine and $Fe^{3+}/Fe^{2+}$ ratio in clinopyroxene change accounting for the $fO_2$ decrease in closed system. This should be taken into account when studying carbonated magmas and magmatic skarns.

Application of thermo-barometric equations available in the literature to carbonated experimental products shows that the most suitable ones are those designed for dry systems (either clinopyroxene alone or anhydrous system). Providing this is due to the well-known effect of $CO_2$ on water activity, it is clear that new barometric

Please cite this article as: Mollo, S., et al., Carbonate assimilation in magmas: A reappraisal based on experimental petrology, Lithos (2009), doi:10.1016/j.lithos.2009.10.013

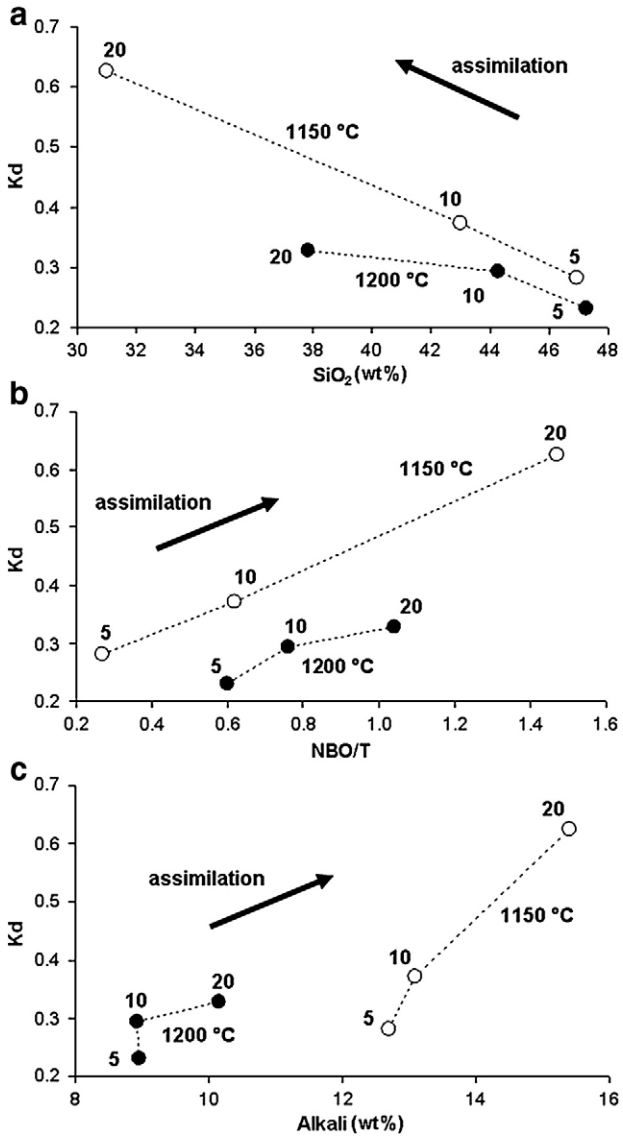


**Fig. 7.** $^{Ol\text{-}melt}Kd_{Fe-Mg}$ (Kd) variation as a function of a) $SiO_2$ content, b) NBO/T ratio (Non-Bridging Oxygen/Tetrahedra), and c) alkalis amount. Numbers (5, 10, and 20) refer to the wt.% of $CaCO_3$ added to the charges.

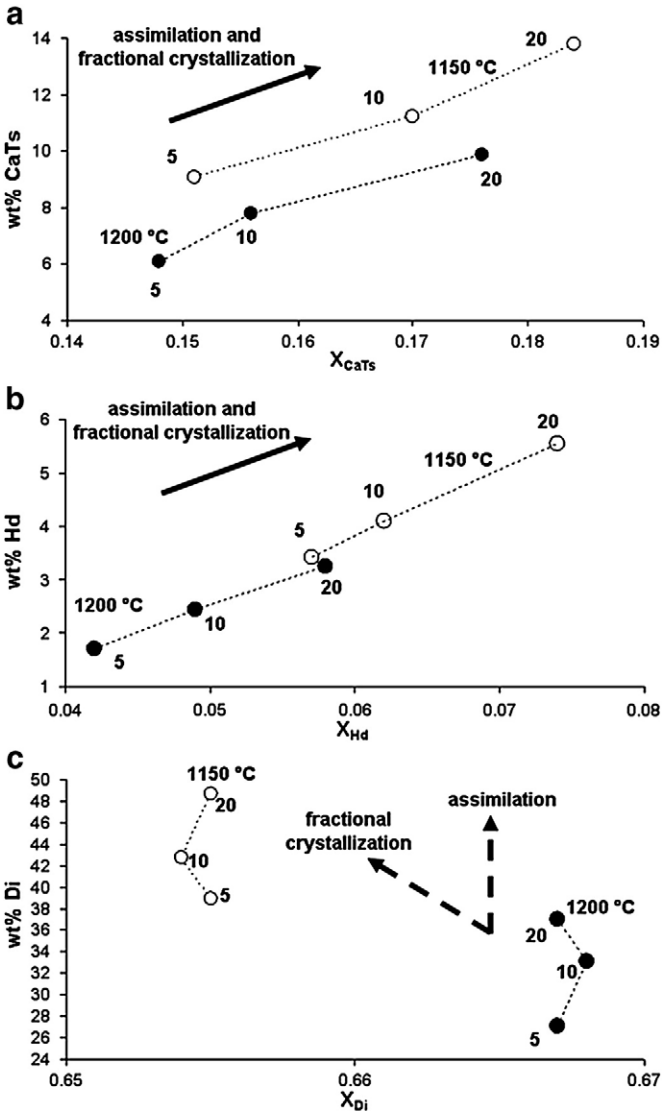


**Fig. 8.** Wt.% components of experimental clinopyroxene plotted versus respective molar fraction. The mass is calculated as follow: total amount of clinopyroxene (in wt.%, Table 1) times molar fraction of Ca-Tschermak, hedenbergite, and diopside component (Table3). a) Ca-Tschermak (CaTs) vs. $X_{CaTs}$. b) Hedenbergite (Hd) vs. $X_{Hd}$. c) Diopside (Di) vs. $X_{Di}$. Numbers (5, 10, and 20) in figure refer to the wt.% of $CaCO_3$ added to the charge.

equations based on mineral–liquid equilibria, in order to be applied on carbonated systems, must be formulated accounting for the important role played by $CO_2$ in magmatic systems.

## Acknowledgments

The authors are grateful to A. Cavallo for assistance during electron microprobe analysis, to H. Behrens for his collaboration during the preparation of starting material. C. Barnes and an anonymous reviewer are thanked for their helpful review of the manuscript. We also acknowledge A. Kerr for his comments and M.J. Heap for his correction to the English text. We benefited from "EU FP6 Research Infrastructure — Transnational Access Programme (RITA)" of the Bayerisches Geoinstitut of Bayreuth (Prof. C. McCammon). This work was supported by TRIGS Project "Sixth Framework Programme of the European Commission and to the New and Emerging Science and Technology Pathfinder" (SM) and by Project FIRB MIUR "Development of innovative technologies for the environmental protection from natural events" (VM).

## References

Barnes, C., Prestvik, T., Sundvoll, B., Surratt, D., 2005. Pervasive assimilation of carbonate and silicate rocks in the Hortavaer igneous complex, north-central Norway. Lithos 80, 179–199.

Beard, J.S., Ragland, P.C., Crawford, M.L., 2005. Reactive bulk assimilation: a model for crustal–mantle mixing in silicic magmas. Geology 33, 681–684.

Behrens, H., Misiti, V., Freda, C., Vetere, F., Botcharnikov, R.E., Scarlato, P., 2009. Solubility of $H_2O$ and $CO_2$ in ultrapotassic melts at 1200 and 1250 °C and pressure from 50 to 500 MPa. American Mineralogist 94, 105–120.

Botcharnikov, R.E., Freise, M., Holtz, F., Behrens, H., 2005a. Solubility of C–O–H mixtures in natural melts: new experimental data and application range of recent models. Annals of Geophysics 48, 633–646.

Botcharnikov, R.E., Holtz, F., Behrens, H., Freise, M., 2005b. The effect of redox state on the solubility of C–O–H fluids in silicate melts: new experimental evidences. EGU05-A-09237.

Please cite this article as: Mollo, S., et al., Carbonate assimilation in magmas: A reappraisal based on experimental petrology, Lithos (2009), doi:10.1016/j.lithos.2009.10.013

**Table 5**
Representative electron microprobe analyses of interstitial glasses (normalised) and clinopyroxene from glass-bearing magmatic skarns (Colli Albani).

| Sample | CA 2a | | AH3AX10 | | AH3AX12 | | AH3AX15 | | AH3AX18 | |
|---|---|---|---|---|---|---|---|---|---|---|
| *Interstitial glass* | | | | | | | | | | |
| wt.% | | sd(2) | | sd(8) | | sd(7) | | sd(11) | | sd(4) |
| $SiO_2$ | 40.24 | 1.14 | 45.18 | 0.32 | 43.74 | 1.27 | 39.72 | 1.14 | 44.58 | 0.47 |
| $TiO_2$ | 0.32 | 0.02 | 0.73 | 0.14 | 1.04 | 0.04 | 0.66 | 0.11 | 0.71 | 0.05 |
| $Al_2O_3$ | 16.80 | 0.45 | 18.46 | 0.26 | 17.54 | 1.08 | 18.71 | 1.50 | 18.12 | 0.34 |
| FeO | 5.70 | 0.15 | 8.70 | 0.82 | 8.68 | 0.48 | 3.30 | 0.38 | 7.14 | 0.23 |
| MnO | 0.39 | 0.06 | 0.19 | 0.03 | 0.16 | 0.02 | 0.12 | 0.04 | 0.16 | 0.02 |
| MgO | 5.87 | 0.43 | 3.74 | 0.17 | 5.12 | 0.95 | 6.15 | 0.85 | 3.78 | 0.08 |
| CaO | 20.92 | 0.52 | 11.58 | 0.82 | 14.12 | 1.99 | 19.33 | 2.72 | 13.96 | 0.22 |
| $Na_2O$ | 2.77 | 0.01 | 2.31 | 0.12 | 1.92 | 0.81 | 2.92 | 0.18 | 2.85 | 0.07 |
| $K_2O$ | 5.90 | 0.43 | 8.30 | 0.35 | 7.03 | 1.09 | 7.70 | 1.41 | 8.07 | 0.24 |
| $P_2O_5$ | 1.09 | 0.02 | 0.81 | 0.06 | 0.65 | 0.09 | 1.39 | 0.01 | 0.63 | 0.04 |
| Total | 100.00 | | 100.00 | | 100.00 | | 100.00 | | 100.00 | |
| Total[a] | 95.87 | | 98.98 | | 98.37 | | 99.87 | | 95.65 | |
| *Clinopyroxene* | | | | | | | | | | |
| wt.% | | sd(6) | | sd(5) | | sd(30) | | sd(8) | | sd(7) |
| $SiO_2$ | 48.89 | 1.38 | 47.63 | 0.35 | 47.67 | 1.00 | 49.04 | 0.27 | 47.67 | 0.53 |
| $TiO_2$ | 0.48 | 0.14 | 0.88 | 0.22 | 1.02 | 0.22 | 0.79 | 0.13 | 0.35 | 0.06 |
| $Al_2O_3$ | 7.47 | 1.74 | 7.56 | 0.36 | 8.31 | 0.64 | 8.54 | 0.34 | 8.40 | 0.60 |
| FeO | 3.90 | 0.59 | 6.35 | 0.96 | 4.74 | 1.39 | 2.36 | 0.05 | 3.76 | 0.24 |
| MnO | 0.09 | 0.03 | 0.06 | 0.03 | 0.05 | 0.03 | 0.03 | 0.02 | 0.05 | 0.03 |
| MgO | 13.92 | 0.82 | 13.15 | 0.46 | 12.97 | 0.83 | 14.77 | 0.20 | 13.56 | 0.32 |
| CaO | 25.18 | 0.22 | 24.43 | 0.26 | 24.79 | 0.40 | 25.49 | 0.24 | 24.93 | 0.31 |
| $Na_2O$ | 0.12 | 0.04 | 0.13 | 0.02 | 0.11 | 0.05 | 0.10 | 0.03 | 0.13 | 0.02 |
| $K_2O$ | 0.02 | 0.01 | 0.02 | 0.02 | 0.01 | 0.01 | 0.01 | 0.01 | 0.01 | 0.01 |
| Total | 100.07 | | 100.21 | | 99.67 | | 101.13 | | 98.85 | |
| *Thermo-barometric results* | | | | | | | | | | |
| *P* (GPa) | 0.25 | | 0.25 | | 0.32 | | 0.29 | | 0.31 | |
| *T* (°C) | 1118 | | 1087 | | 1114 | | 1126 | | 1081 | |

Pressure and temperature crystallization conditions were estimated by applying equations 32a in Putirka (2008) and T1 in Putirka et al. (1996), respectively. sd represents the standard deviation (in parenthesis number of averaged analyses).
[a] WDS-EMP total.

2007. Carbonate assimilation at Merapi Volcano, Java, Indonesia: insights from crystal isotope stratigraphy. Journal of Petrology 48, 1793–1812.
Cheadle, M.J., Elliott, M.T., McKenzie, D., 2004. Percolation threshold and permeability of crystallizing igneous rocks: the importance of textural equilibrium. Geology 32, 757–760.
Conte, A.M., Dolfi, D., Gaeta, M., Misiti, V., Mollo, S., Perinelli, C., 2009. Experimental constraints on evolution of leucite–basanite magma at 1 and 10–4 GPa: implications for parental compositions of Roman high-potassium magmas. European Journal of Mineralogy 21, 763–782.
Coulson, I.M., Westphal, M., Anderson, R.G., Kyser, T.K., 2007. Concomitant skarn and syenitic magma evolution at the margins of the Zippa Mountain pluton. Mineralogy and Petrology 90, 199–221.

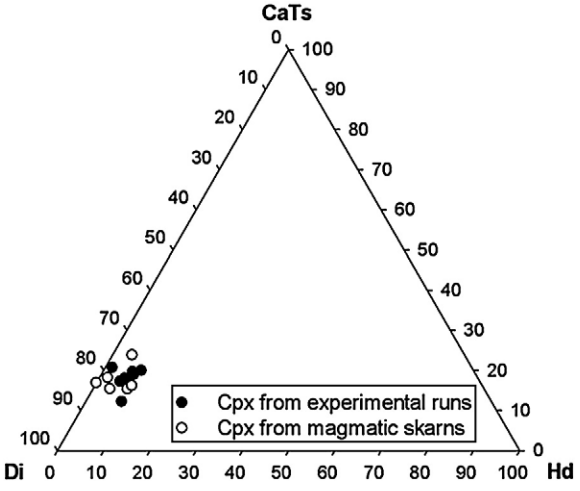


**Fig. 9.** Diopside–hedenbergite–Ca-Tschermak (molar fraction) diagram. Molar fraction of clinopyroxenes from magmatic skarns (Table 6) is compared with molar fraction of experimental clinopyroxenes (Table 3).

anhydrous near-solidus peridotite melts at 1 GPa. Earth and Planetary Science Letters 152, 149–162.
Freda, C., Gaeta, M., Misiti, V., Mollo, S., Dolfi, D., Scarlato, P., 2008. Magma–carbonate interaction: an experimental study on ultrapotassic rocks from Alban Hills (Central Italy). Lithos 101, 397–415.
Fulignati, P., Marianelli, P., Santacroce, R., Sbrana, A., 2004. Probing the Vesuvius magma chamber–host rock interface through xenoliths. Geological Magazine 141, 417–428.
Gaeta, M., Freda, C., Christensen, J.N., Dallai, L., Marra, F., Karner, D.B., Scarlato, P., 2006. Time-dependent geochemistry of clinopyroxene from Alban Hills (Central Italy): clues to source and evolution of ultrapotassic magmas. Lithos 86, 330–346.
Gaeta, M., Di Rocco, T., Freda, C., 2009. Carbonate assimilation in open magmatic systems: the role of melt-bearing skarns and cumulate-forming processes. Journal of Petrology

**Table 6**
Standard error of estimate (SEE) for pressure and temperature calculated by applying different thermo-barometric equations to 72 clinopyroxene–melt couples from hydrous-carbonated experiments.

| | Equation | SEE |
|---|---|---|
| *Pressure calculation* | | |
| Models based on clinopyroxene–melt equilibrium | P1 in Putirka et al., 1996 | 1.47 |
| | Putirka et al., 2003 | 3.28 |
| | 30 in Putirka, 2008 | 5.54 |
| | 31 in Putirka, 2008 | 5.87 |
| | 32c in Putirka, 2008 | 6.32 |
| Models based on clinopyroxene alone | Nimis, 1995 | 1.4 |
| | Nimis and Ulmer, 1998 | 1.42 |
| | 32a in Putirka, 2008 | 1.06 |
| | 32b in Putirka, 2008 | 1.1 |
| *Temperature calculation* | | |
| Models based on clinopyroxene–melt equilibrium | T3 Putirka et al., 1996 | 104.18 |
| | T1 Putirka et al., 1996 | 33.93 |
| | Putirka et al., 2003 | 50.72 |
| | 33 Putirka, 2008 | 50.48 |
| | 34 Putirka, 2008 | 34.34 |
| | 32d Putirka, 2008 | 56.09 |

Please cite this article as: Mollo, S., et al., Carbonate assimilation in magmas: A reappraisal based on experimental petrology, Lithos (2009), doi:10.1016/j.lithos.2009.10.013

Holness, M.B., 2005. Melt–solid dihedral angles of common minerals in natural rocks. Journal of Petrology 47, 791–800.
Iacono Marziano, G., Gaillard, F., Pichavant, M., 2008. Limestone assimilation by basaltic magmas: an experimental re-assessment and application to Italian volcanoes. Contributions to Mineralogy and Petrology 155, 719–738.
Kadik, A., Pineau, F., Litvin, Y., Jendrzejewski, N., Martinez, I., Javoy, M., 2004. Formation of carbon and hydrogen species in magmas at low oxygen fugacity. Journal of Petrology 45, 1297–1310.
Kamenetsky, V., Metrich, N., Cioni, R., 1995. Potassic primary melts of Vulsini (Roman Province): evidence from mineralogy and melt inclusions. Contributions to Mineralogy and Petrology 120, 186–196.
Kawamoto, T., Hirose, K., 1994. Au–Pd sample containers of melting experiments on iron and water-bearing systems. European Journal of Mineralogy 6, 381–385.
Kerrick, D.M., 1977. The genesis of zoned skarns in the Sierra Nevada, California. Journal of Petrology 18, 144–181.
Kress, V.C., Carmichael, I.S.E., 1991. The compressibility of silicate liquids containing $Fe_2O_3$ and the effect of composition, temperature, oxygen fugacity and pressure on their redox states. Contributions to Mineralogy and Petrology 108, 82–92.
Kushiro, I., 1990. Partial melting of mantle wedge and evolution of island arc crust. Journal of Geophysical Research 95, 15929–15939.
Kushiro, I., Mysen, B.O., 2002. A possible effect of melt structure on the Mg–$Fe^{2+}$ partitioning between olivine and melt. Geochimica et Cosmochimica Acta 66, 2267–2272.
Kushiro, I., Walter, M.J., 1998. Mg–Fe partitioning between olivine and mafic–ultramafic melts. Geophysical Research Letters 25, 2337–2340.
Longhi, J., Walker, D., Hays, J.F., 1978. The distribution of Fe and Mg between olivine and lunar basaltic liquids. Contributions to Mineralogy and Petrology 42, 1545–1558.
Nimis, P., 1995. A clinopyroxene geobarometer for basaltic systems based on crystal-structure modeling. Contributions to Mineralogy and Petrology 121, 115–125.
Nimis, P., Ulmer, P., 1998. Clinopyroxene geobarometry of basic magmas: an expanded structural geobarometer for anhydrous and hydrous systems. Contributions to Mineralogy and Petrology 133, 122–135.
O'Neill, H.St.C., Eggins, S.M., 2002. The effect of melt composition on trace element partitioning: an experimental investigation of the activity coefficients of FeO, NiO, CoO, $MoO_2$ and $MoO_3$ in silicate melts. Chemical Geology 186, 151–181.
Peccerillo, A., 2005. The Roman Province. In: Springer Berlin Heidelberg (Ed.), Plio-Quaternary Volcanism in Italy. Springer New York.
Putirka, K., 1999. Clinopyroxene + liquid equilibria. Contributions to Mineralogy and Petrology 135, 151–163.
Putirka, K.D., 2008. Thermometers and barometers for volcanic systems. In: Putirka, K.D., Tepley, F. (Eds.), Minerals, Inclusions, and Volcanic Processes: Review in Mineralogy and Geochemistry, vol. 69, pp. 61–120.
Putirka, K., Johnson, M., Kinzler, R., Walker, D., 1996. Thermobarometry of mafic igneous rocks based on clinopyroxene–liquid equilibria, 0–30 kbar. Contributions to Mineralogy and Petrology 123, 92–108.
Putirka, K., Ryerson, F.J., Mikaelian, H., 2003. New igneous thermobarometers for mafic and evolved lava compositions, based on clinopyroxene + liquid equilibria. American Mineralogist 88, 1542–1554.
Roeder, P.L., Emslie, R.F., 1970. Olivine–liquid equilibrium. Contributions to Mineralogy and Petrology 29, 275–289.
Rogers, N.W., Hawkesworth, C.J., Parker, R.J., March, J.S., 1985. The geochemistry of potassic lavas from Vulsini, central Italy and implications for mantle enrichment processes beneath the Roman region. Contributions to Mineralogy and Petrology 90, 244–257.
Sack, R.O., Walker, D., Carmichael, I.S.E., 1987. Experimental petrology of alkalic lavas: constraints on cotectics of multiple saturation in natural basic liquids. Contributions to Mineralogy and Petrology 96, 1–23.
Schuessler, J.A., Botcharnikov, R.E., Behrens, H., Misiti, V., Freda, C., 2008. Oxidation state of iron in phonotephritic melts. American Mineralogist 93, 1493–1504.
Sugawara, T., 1998. Review on element partitioning for olivine-liquid and plagioclase-liquid. Bulletin of the Volcanological Society of Japan 43, 181–201.
Toplis, M.J., 2005. The thermodynamics of iron and magnesium partitioning between olivine and liquid: criteria for assessing and predicting equilibrium in natural and experimental systems. Contributions to Mineralogy and Petrology 149, 22–39.
Wenzel, T., Baumgartner, L.P., Brugmann, G.E., Konnikov, E.G., Kislov, E.V., 2002. Partial melting and assimilation of dolomitic xenoliths by mafic magma: the Ioko–Dovyren intrusion (North Baikal Region, Russia). Journal of Petrology 43, 2049–2074.

Please cite this article as: Mollo, S., et al., Carbonate assimilation in magmas: A reappraisal based on experimental petrology, Lithos (2009), doi:10.1016/j.lithos.2009.10.013